

## Crystal structures and compositions of sanidine and high albite in cryptoperthitic intergrowth

KEITH D. KEEFER AND GORDON E. BROWN

Department of Geology, Stanford University  
Stanford, California 94305

### Abstract

The crystal structures and compositions of the phases in a natural cryptoperthite from the Rabb Canyon pegmatite, Grant County, New Mexico, have been determined using single-crystal X-ray diffraction, transmission electron microscopy, and electron microprobe analysis. The cryptoperthite consists of an untwinned, monoclinic sanidine [cell dimensions:  $a = 8.558(1)$ ,  $b = 12.997(1)$ ,  $c = 7.179(1)\text{Å}$ ,  $\beta = 116.07^\circ(1)$ ] and a pericline-twinned, triclinic high albite [cell dimensions:  $a = 8.144(2)$ ,  $b = 12.989(3)$ ,  $c = 7.160(2)\text{Å}$ ,  $\alpha = 92.10^\circ(2)$ ,  $\beta = 116.56(2)^\circ$  and  $\gamma = 90.21(2)^\circ$ ]. The similarity of the  $b$  and  $c$  cell dimensions and precession X-ray photographs indicate that the phases are partially, but not completely, coherent in the intergrowth plane,  $\sim(601)$ . The bulk composition of the crystal determined by microprobe analysis is  $\text{Or}_{0.51}\text{Ab}_{0.48}\text{An}_{0.01}$ , and the mole fraction of the sanidine phase in the crystal determined by X-ray scale factor refinement is 0.68(1). TEM examination showed that the high-albite lamellae are  $\sim 500\text{Å}$  wide with  $\sim 50\text{Å}$ -wide pericline twin lamellae. The sanidine lamellae are  $\sim 1000\text{Å}$  wide. The composition of the sanidine phase, as determined by direct crystallographic site refinement, is  $\text{Or}_{0.65(1)}\text{Ab}_{0.35}$ . The composition of the high-albite phase, as determined by mass-balance, is  $\text{Or}_{0.22(2)}\text{Ab}_{0.78}$ .

Both phases in this cryptoperthite are strained, although the nature and amount of strain differ from predictions of models of elastic strain in perfectly coherent feldspars. No previously-reported method of predicting the composition of the phases in a cryptoperthite from the cell dimensions yields correct results for this specimen. The observed compositions lie on an experimentally-determined coherent solvus at a temperature of  $465 \pm 20^\circ$ .

### Introduction

Cryptoperthites are submicroscopic intergrowths of sodic and potassic alkali feldspars resulting from exsolution of a homogeneous feldspar of intermediate composition. The unit-cell dimensions of the intergrown phases commonly differ significantly from those of compositionally-similar non-intergrown phases (Stewart and Wright, 1974). This discrepancy is attributed to elastic strain induced by preservation of a partially to completely coherent aluminosilicate framework across the phase boundary during exsolution (Owen and McConnell, 1974; Yund, 1974). Efforts to determine the amount of strain and how it affects exsolution have been hampered by the difficulty of determining the composition of the exsolved lamellae, which are too small to be chemically analyzed with an electron microprobe. The compositions of such intergrown phases are commonly estimated

from the cell volumes (Stewart and Wright, 1974). Cell volumes are, however, affected by elastic strain and thus do not yield a correct estimate of compositions for coherent cryptoperthite. Robin (1974) and Tullis (1975) have developed methods for correcting these compositional estimates by calculating the elastic strain of the unit cell caused by coherency. However, their corrections apply only in the case of complete coherency of monoclinic phases, and they have not been verified experimentally. Previous attempts to refine the crystal structures of the individual phases of a cryptoperthite have not been wholly successful because of the difficulties in resolving the diffraction maxima of the intergrown phases, one or both of which are usually twinned (Ribbe and Gibbs, 1975).

In this study, both intergrown phases of a cryptoperthite were examined by single-crystal X-ray diffraction and transmission electron microscopy with

the following objectives: (1) to develop techniques by which the structures of the phases in such an intergrowth may be determined; (2) to determine the composition of the individual phases using X-ray diffraction techniques and data on the bulk composition; (3) to investigate the structural changes caused by partial coherency; and (4) to use these data as a basis upon which to evaluate methods of determining the composition and amount of strain of the phases in cryptoperthite from the cell dimensions.

### Experimental

The material used in this study came from the Rabb Canyon pegmatite, Grant County, New Mexico (Kuellmer, 1954). The pegmatite occurs in porphyry that is the vent facies of a rhyolite dome (J. O'Brien, personal communication, 1976). The cryptoperthite occurs in a matrix of coarsely crystalline quartz as clear, colorless single-crystal fragments about 1cm in diameter, which display perfect cleavage parallel to (010) and (001).

Precession X-ray photographs of a specimen ( $0.34 \times 0.20 \times 0.14$ mm) taken from a crystal fragment show that the cryptoperthite consists of an untwinned, monoclinic sanidine phase and a pericline-twinned, triclinic high-albite phase<sup>1</sup> (Fig. 1). The majority of diffraction maxima from both phases are distinct and generally well resolved, although slight streaking between the maxima is observed. This crystal was later used for integrated intensity measurements on the intergrown phases. A transmission electron micrograph of the material is shown in Figure 2.

All measurements of the X-ray diffraction intensities were made on a Picker FACS-1 four-circle diffractometer with graphite monochromatized  $\text{MoK}\alpha$  radiation ( $\lambda = 0.71069\text{\AA}$ ). The unit-cell dimensions at  $23^\circ\text{C}$  of all three lattices were determined by least-squares fit to the angular coordinates of reflections centered by the FACS-1 programs. Eighteen reflections in the range  $12\text{--}49^\circ 2\theta$  were used for the sanidine phase and 15 reflections in the range  $12\text{--}49^\circ 2\theta$  were used for each of the high-albite twins. The cell dimensions of the high-albite twins differ by less than one standard deviation. The observed cell dimensions are given in Table 1, together with cell dimensions calculated from the observed composi-

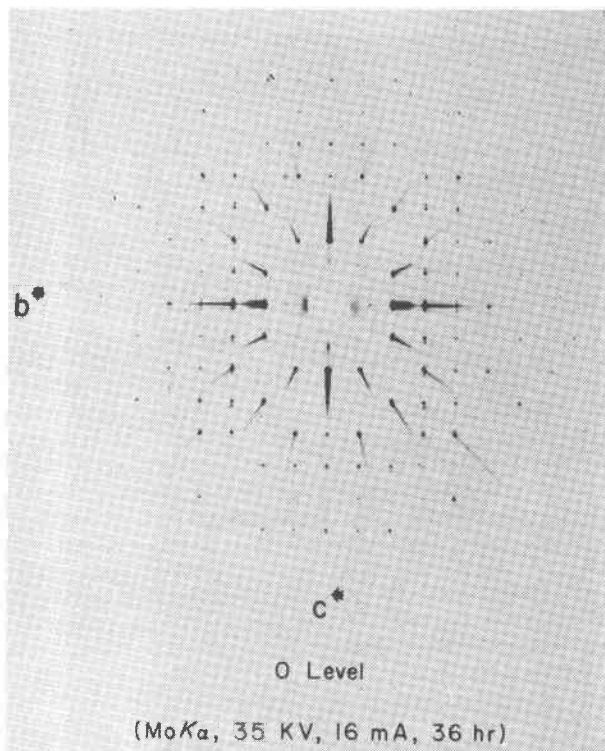


Fig. 1. Zero-level precession X-ray photograph ( $\text{MoK}\alpha$  radiation) of the  $b^*c^*$  net of the cryptoperthite. The most intense lattice is that of sanidine. The two less intense lattices are those of high-albite twins.

tions using Luth and Querol-Suñé's (1970) regression equations.

Precession photographs show that the space group of the sanidine phase is  $C2/m$  ( $hkl$  systematically absent when  $h + k = 2n + 1$ ). The high-albite phase was referred to the nonstandard space group  $C\bar{1}$  ( $hkl$  systematically absent when  $h + k = 2n + 1$ ) which is conventionally used for triclinic feldspars to facilitate comparison of the monoclinic and triclinic structures.

Integrated intensities in the range  $5\text{--}60^\circ 2\theta$  were measured for the sanidine phase with a  $\theta\text{--}2\theta$  scan at a  $1^\circ/\text{min}$  scan rate using a  $1.5^\circ$  take-off angle and a  $2.6^\circ 2\theta$  scan width compensated for  $\alpha_1\text{--}\alpha_2$  splitting. Backgrounds were estimated from 20-second counts made at each end of the scan. Intensities in the range  $30\text{--}75^\circ 2\theta$  were measured for one of the high-albite twins using a  $0.5^\circ/\text{min}$  scan rate, a  $2.3^\circ 2\theta$  scan width, and 100-second background counts. Other conditions were the same as those used for data collection on the sanidine phase.

The diffraction intensities from each lattice in the range  $40\text{--}45^\circ 2\theta$  (160 observations for the sanidine and 270 for each of the high-albite twins) were remea-

<sup>1</sup> The terms sanidine and high albite refer to potassic and sodic feldspars, respectively, in which the Al-Si distribution among the non-equivalent tetrahedral sites is nearly fully disordered. A pericline twin is a rotation twin with a twin axis of [010] and a composition plane near (001), the so-called rhombic section.

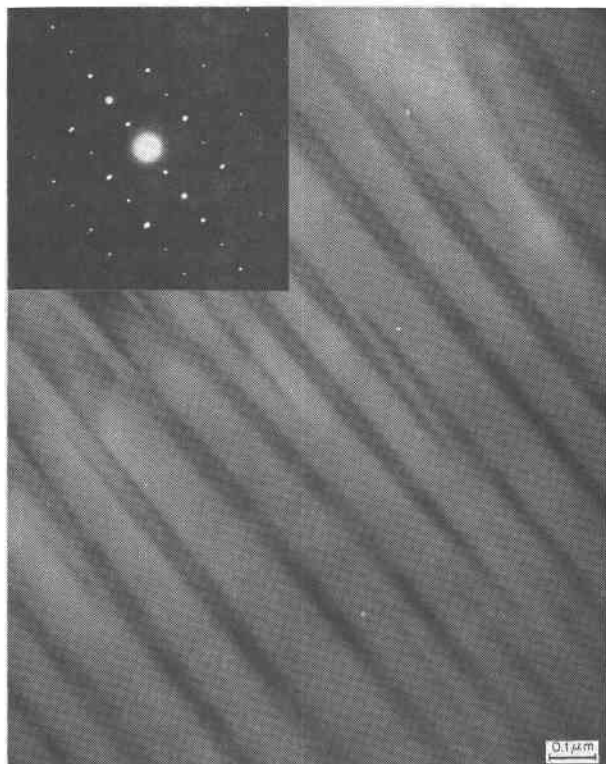


Fig. 2. Bright-field transmission electron micrograph of a section from the fragment cut parallel to the (001) cleavage plane. The sanidine lamellae have a maximum width of 1000Å and alternate regularly with high-albite lamellae whose maximum width is 500Å. The intergrowth plane is approximately parallel to  $(\bar{0}01)$  and normal to this section. Micrographs were made on a 100 kV Philips 200 microscope in the Department of Materials Science and Engineering at the University of California, Berkeley.

sured using identical instrument settings. These observations were used to determine the relative amounts of each phase in the sample, as discussed below. The intensities from each high-albite twin were the same to within 0.1 percent, confirming that both twins have the same structure and are present in equal amounts.

Observed intensities were corrected for background, Lorentz, and polarization effects, the latter assuming a 50 percent mosaic monochromator crystal. The observations were scaled to normalized standard observations to correct for instrument drift; maximum and minimum scaling factors were 1.03 and 0.96, respectively. Corrections for absorption were made using an analytical method<sup>2</sup> ( $\mu = 8.0 \text{ cm}^{-1}$ , calculated from the bulk composition of the crystal; minimum and maximum transmissions were 0.91 and 0.95, respectively). Standard deviations were estimated using the formula of Corfield *et al.* (1967), which employs an instrumental instability constant of 0.04.

The crystal used in the diffraction experiment was analyzed with an electron microprobe. The bulk composition was: (weight percent) 66.81 SiO<sub>2</sub>, 18.67 Al<sub>2</sub>O<sub>3</sub>, 8.91 K<sub>2</sub>O, 5.39 Na<sub>2</sub>O, 0.20 CaO, 0.13 FeO, corresponding to Or<sub>0.51</sub>Ab<sub>0.48</sub>An<sub>0.01</sub>.

<sup>2</sup> Using the formula of De Meulenaer and Tompa (1965) in the program AGNOST. Programs used for other calculations were A. Zalkin's FORDAP, a modified version of Finger's RFINE, and locally-written programs by K. Keefe for reducing and correcting the data.

Table 1. Comparison of observed and calculated cell parameters for sanidine and high albite in cryptoperthitic intergrowth

	SANIDINE				HIGH ALBITE					
	Observed	Calculated	$\Delta^2$	Strain(%)	Observed	Calculated	$\Delta$	Strain(%)	$\Delta\text{OBS}^3$	$\Delta\text{CALC}^4$
$a(\text{\AA})$	8.558(1) <sup>1</sup>	8.452(5)	0.106	1.25	8.144(2)	8.248(8)	-0.104	-1.26	0.414	0.204
$b(\text{\AA})$	12.997(1)	13.004(1)	-0.007	-0.05	12.989(3)	12.932(6)	0.057	0.44	0.008	0.072
$c(\text{\AA})$	7.179(1)	7.169(1)	0.010	0.14	7.160(2)	7.140(3)	0.020	0.28	0.019	0.029
$\alpha(^{\circ})$	90.00	90.00	0.00		92.10(2)	92.05(18)	0.05		-2.10	-2.05
$\beta(^{\circ})$	116.07(1)	116.07(1)	0.00		116.56(2)	116.37(1)	0.19		-0.48	-0.30
$\gamma(^{\circ})$	90.00	90.00	0.00		90.21(2)	90.20(2)	0.01		-0.21	-0.20
$V(\text{\AA}^3)$	717.2	708.0	9.2	1.30	676.9	681.7	-4.8	-0.70	40.3	26.3

<sup>1</sup>Number in parentheses are e.s.d.'s ( $1\sigma$ ) in the least significant digits.

<sup>2</sup> $\Delta$  = observed - calculated

<sup>3</sup> $\Delta\text{OBS}$  = OBS(SANIDINE) - OBS(HIGH ALBITE)

<sup>4</sup> $\Delta\text{CALC}$  = CALC(SANIDINE) - CALC(HIGH ALBITE)

### Structure refinement

Strip-chart recording of diffraction maxima during the intensity measurements did not permit unequivocal determination of interference among diffraction maxima from the three lattices. Therefore, the differences in the  $\chi$ ,  $\omega$ , and  $2\theta$  instrument-setting angles between any reciprocal lattice point under observation and the nearest one of each of the other two lattices were calculated. An observation was excluded from the refinement if all three angular differences were less than the instrumental resolution ( $1.2^\circ$  in  $\chi$ ,  $0.5^\circ$  in  $\omega$ , and  $1^\circ$  in  $2\theta$ ). In the  $h0l$ ,  $h \pm 1l$ , and  $h \pm 2l$  zones, many points in the high-albite reciprocal lattice were very narrowly separated from points in the twin lattice. If the angular separation of points was sufficiently small to assure that both diffracted intensities were measured completely in a single observation, such an observation was included in the refinement and treated as follows.

Because both high-albite twins have the same structure, a single observation which includes more than one intensity from different twins may be treated as a combination of different intensities from the same twin. If the individual diffracted rays do not interfere, the intensity of the combination is given by the equation:

$$I = k \sum F_i^2$$

where  $I$  is the combined, unresolved intensity,  $F_i$  are the structure factors of the contributing diffraction maxima and  $k$  is a constant which includes the  $L_p$  factors, absorption corrections, and a scaling factor. (The differences among the  $L_p$  and absorption factors that would have then applied to the  $F_i$  individually are negligible.) For the case in which the intensity is due to a single diffraction maximum, least-squares refinement requires evaluation of derivatives of the form:

$$\frac{\partial(I/k)^{1/2}}{\partial P_j} = \frac{\partial|F|}{\partial P_j} = F^{-1} \left( \frac{\partial A}{\partial P_j} + \frac{\partial B}{\partial P_j} \right)$$

where  $A$  and  $B$  are the real and imaginary parts of the structure factor and  $P_j$  are the parameters being varied. For refinement on combined intensities, these derivatives may be computed from the equation:

$$\frac{\partial(I/k)^{1/2}}{\partial P_j} = \frac{\partial(\sum F_i^2)^{1/2}}{\partial P_j} = \left( \sum_i F_i^2 \right)^{-1/2} \sum_i \left( A_i \frac{\partial A_i}{\partial P_j} + B_i \frac{\partial B_i}{\partial P_j} \right)$$

The full-matrix least-squares program RFINE (Finger

and Prince, 1975) was modified to calculate these derivatives for combined intensities.

The initial model used in the least-squares refinement of the sanidine structure was the feldspar structure reported by Fenn and Brown (1977). The neutral atom form factors of Cromer and Mann (1968) were employed, and complete disorder of the Al/Si distribution ( $\text{Si}_{0.75}\text{Al}_{0.25}$ ) in the tetrahedral sites was assumed. Refinement converged after 10 cycles with anisotropic thermal parameters and an alkali-site occupancy of  $\text{K}_{0.8}\text{Na}_{0.2}$  [estimated from the Tullis (1975) model]. The alkali-site occupancy was then refined for 7 more cycles to yield  $\text{K}_{0.65 \pm 0.02}\text{Na}_{0.35}^3$  with the constraint that the total site occupancy be 1.00. Refinement was performed on  $F$  using weights of  $1/\sigma_F^2$ . 140 observations were excluded from the refinement on the basis of the resolution calculation, and 13 other observations were rejected because  $F/\sigma_F > 8$ , leaving a total of 924 observations in the final sanidine refinement (Table 2a)<sup>4</sup>. The final conventional  $R = 0.029$  ( $R = 0.033$  including observations rejected because of poor fit), weighted  $R_w = 0.039$  [ $R_w = [\sum w(|F_o| - |F_c|)^2 / \sum w |F_o|^2]^{1/2}$ ], and the standard deviation of a unit weight observation was 1.56. Because of the importance of the refined sanidine K/Na occupancy in our calculation of the composition of the albite phase, an analysis of weights was performed. Weights of  $1/\sigma_F^2$  gave essentially equal values of  $(\Delta F/\sigma)$  for equal-sized groups of  $F_{\text{obs}}$  and hence are preferable to a non-statistical weighting scheme. Positional parameters are given in Table 3a.

The initial model used in the high-albite refinement was the structure reported by Ribbe *et al.* (1969), with the same form factors and tetrahedral site occupancies that were used in the sanidine refinement. A single alkali site with an occupancy of  $\text{Na}_{0.9}\text{K}_{0.1}$  was assumed. After convergence of refinement with anisotropic temperature factors, the much poorer fit of observations at larger values of  $\sin\theta/\lambda$  coupled with residual electron density in a difference Fourier synthesis suggested that a model with a disordered alkali site might be more appropriate than a model with a single alkali atom position. Both the two-site, half-atom model of Ribbe *et al.* (1969) and the four-site,

<sup>3</sup> The quoted error is  $\pm 2\sigma$ , a convention used throughout the paper.

<sup>4</sup> Structure factor tables for both refinements have been placed on deposit. To receive a copy of Table 2 order document AM-78-079 from the Business Office, Mineralogical Society of America, 1909 K Street N.W., Washington, D.C. 20006. Please remit \$1.00 in advance for the microfiche.

Table 3a. Sanidine fractional coordinates and thermal parameters

Atom	<i>x</i>	<i>y</i>	<i>z</i>	$\beta_{11}^2$	$\beta_{22}$	$\beta_{33}$	$\beta_{12}$	$\beta_{13}$	$\beta_{23}$
M	0.2844(1) <sup>1</sup>	0.0000	0.1383(1)	51(1)	45(1)	118(2)	0	23(1)	0
T <sub>1</sub>	0.0091(1)	0.1834(1)	0.2236(1)	49(1)	19(1)	35(1)	-4(1)	22(1)	-2(1)
T <sub>2</sub>	0.7069(1)	0.1177(1)	0.3431(1)	46(1)	14(1)	45(1)	-1(1)	20(1)	0(1)
O <sub>A1</sub>	0.0000	0.1443(2)	0.0000	104(3)	31(1)	76(4)	0	50(3)	0
O <sub>A2</sub>	0.6308(3)	0.0000	0.2832(3)	87(3)	19(1)	113(5)	0	21(3)	0
O <sub>B</sub>	0.8270(2)	0.1448(1)	0.2255(2)	78(2)	44(1)	120(3)	-9(1)	58(2)	5(1)
O <sub>C</sub>	0.0327(2)	0.3092(1)	0.2568(2)	71(2)	25(1)	98(3)	-5(1)	30(2)	-6(1)
O <sub>D</sub>	0.1814(2)	0.1256(1)	0.4049(2)	80(2)	28(1)	63(3)	2(1)	13(2)	2(1)

<sup>1</sup>Numbers in parentheses are *e.s.d.*'s ( $1\sigma$ ) in the least significant digits.

<sup>2</sup>Thermal parameters ( $\times 10^4$ ) are of the form  $T = \exp(-\sum \sum h_i h_j \beta_{ij})$ .

quarter-atom model of Prewitt *et al.* (1976) were tried; neither gave any significant improvement in the refinement. On the basis of simplicity and ease of interpretation, the single alkali site model was chosen for the final refinement. Several cycles of refinement in which the Na fraction of the alkali site occupancy was varied (the K fraction was constrained so that the total site occupancy was 1.00) failed to produce a chemically reasonable Na fraction. Therefore the alkali site occupancy was fixed at Na<sub>0.8</sub>K<sub>0.2</sub>, based on tentative results of the calculation of the analbite composition described below. Refinement was performed on F with weights of  $1/\sigma_F^2$ , which were found to be satisfactory after making the same analysis as was made of the sanidine weights. Because of the large number of observations, many of which were extremely weak, only observations for which  $F > 3\sigma_F$  were used in the refinement. Of the 2306 observations which met this criterion, 479 were excluded on the basis of the resolution calculation and 129 were rejected because  $\Delta F/\sigma_F > 8$ , leaving a total of 1698 observations in the final cycle of refinement (Table 2b). The final conventional  $R = 0.083$  ( $R = 0.107$  including observations rejected due to poor fit),  $R_w = 0.096$ , and the standard deviation of a unit weight observation was 2.87. Positional parameters are given in Table 3b.

These large residuals and large number of observations rejected due to poor agreement reflect the experimental difficulties encountered in measuring the high-albite intensities. Ninety percent of the  $F_{\text{obs}}$  rejected were much smaller than  $F_{\text{calc}}$ . Although no

experimental source of error could be found, the high-albite twin studied comprised only 16 percent of the total volume of the crystal; thus the effects of any interference of the sanidine intensities with the intensities of the high albite were exacerbated. One likely, although unproven, explanation for this poor agreement is that the structure within each albite lamella may vary in distortion from the intergrowth boundary to the center, resulting in the high thermal parameters reported below. Such a structure would not diffract as well as an undistorted one, and the anisotropic thermal model used does not adequately account for this effect.

### Results

The mole fraction of each phase in the crystal was calculated from the relative diffraction intensities of each phase. The observed X-ray diffraction intensity may be expressed as:

$$I_{\text{obs}} = \epsilon N k F^2$$

where  $N$  is the number of unit cells diffracting,  $k$  is the combined  $L_p$  and absorption correction,  $F$  is the structure factor, and  $\epsilon$  is an instrumental constant which is the same for sets of observations measured under identical experimental conditions. The product  $\epsilon N$  is then the scaling factor used as a parameter in least-squares refinement. These values for each phase were determined by least-squares refinement of the scaling factor of each of the fully refined structures, using observations of each phase measured under identical experimental conditions. The fraction of

unit cells which constitute the sanidine phase may then be calculated from the equation:

$$\text{Fraction of sanidine cells} = \frac{\epsilon N_{\text{sanidine}}}{(\epsilon N_{\text{sanidine}} + 2\epsilon N_{\text{high albite}})}$$

(the factor 2 appears in the denominator because there are two high albite twins). Because  $Z = 4$  for both structures, the result is the mole fraction of the sanidine, found to be  $0.68 \pm 0.02$  for this specimen. This figure is in excellent agreement with an estimate (0.67) derived from the electron micrographs of this material.

As noted above, the composition of the high-albite phase could not be determined by site refinement. However, because the sanidine composition, the mole fractions of sanidine and high albite, and the bulk composition of the crystal are known, the composition of the high-albite phase may be determined by mass-balance. The result obtained is  $\text{Na}_{0.78 \pm 0.05} \text{K}_{0.22} \text{AlSi}_3\text{O}_8$ . The Ca and Fe content of the crystal is neglected, because there is no practical way of estimating the Ca or Fe content of either phase. The bulk  $\text{CaAl}_2\text{Si}_2\text{O}_8$  component determined by microprobe analysis is only 1 percent of total components and the

percent bulk FeO is even less; thus the error due to the neglect of these components is within the estimated errors noted above. The calculated density of the crystal is  $2.55 \text{ g/cm}^3$  and the density determined by flotation is  $2.57 \text{ g/cm}^3$ .

#### The sanidine structure

The structure of the intergrown sanidine phase is virtually identical to the structure of a non-intergrown sanidine of composition  $\text{K}_{0.85} \text{Na}_{0.15} \text{AlSi}_3\text{O}_8$  reported by Phillips and Ribbe (1973). This similarity, reflected by the small differences of the cell dimensions ( $>0.02 \text{ \AA}$ ), is probably coincidental, considering the large difference in composition between the phases. Because no structure has been reported for a non-intergrown sanidine closer in composition to the sanidine examined in this study, there is no reference structure available for ready comparison. Fenn and Brown (1977) found that the mean alkali-oxygen distance,  $\langle \text{M-O} \rangle$ , varies almost linearly with the K content of alkali feldspars containing little or no Ca. For the composition of the sanidine in this study, their results predict an  $\langle \text{M-O} \rangle$   $0.02 \text{ \AA}$  shorter than that observed. This difference is consistent with the elon-

Table 3b. High-albite fractional coordinates and thermal parameters

Atom	x	y	z	$\beta_{11}^2$	$\beta_{22}$	$\beta_{33}$	$\beta_{12}$	$\beta_{13}$	$\beta_{23}$
M	0.2690(4) <sup>2</sup>	0.0048(5)	0.1319(8)	101(4)	143(4)	357(12)	9(3)	26(5)	-113(6)
T <sub>1o</sub>	0.0078(2)	0.1694(1)	0.2182(2)	63(2)	30(1)	36(3)	-2(1)	23(2)	0(1)
T <sub>1m</sub>	0.0057(2)	0.8175(1)	0.2261(2)	59(2)	30(1)	36(3)	6(1)	17(2)	5(1)
T <sub>2o</sub>	0.6893(2)	0.1104(1)	0.3287(2)	50(2)	29(1)	50(3)	0(1)	12(2)	3(1)
T <sub>2m</sub>	0.6857(2)	0.8802(1)	0.3484(2)	51(2)	29(1)	45(3)	3(1)	13(2)	3(1)
O <sub>A1</sub>	0.0035(7)	0.1359(3)	0.9914(8)	125(6)	42(2)	88(8)	-1(3)	59(5)	-3(3)
O <sub>A2</sub>	0.5913(5)	0.9943(3)	0.2821(6)	71(5)	35(2)	91(7)	-2(2)	26(4)	1(3)
O <sub>Bo</sub>	0.8216(6)	0.1145(4)	0.2108(8)	81(6)	54(3)	154(11)	-11(3)	74(7)	-3(4)
O <sub>Bm</sub>	0.8184(6)	0.8552(4)	0.2378(8)	89(6)	61(3)	122(10)	13(3)	48(6)	-1(4)
O <sub>Co</sub>	0.0152(6)	0.2959(3)	0.2658(7)	90(6)	40(2)	97(9)	-10(3)	32(6)	-4(3)
O <sub>Cm</sub>	0.0202(6)	0.6893(3)	0.2329(7)	89(6)	34(2)	96(9)	10(3)	15(5)	6(3)
O <sub>Do</sub>	0.1965(6)	0.1168(3)	0.3950(7)	91(6)	40(2)	77(9)	9(3)	18(5)	8(3)
O <sub>Dm</sub>	0.1918(6)	0.8710(3)	0.4190(7)	100(6)	39(2)	69(8)	-4(3)	-10(5)	-6(3)

<sup>1</sup>Numbers in parentheses are e.s.d.'s ( $1\sigma$ ) in the least significant digits.

<sup>2</sup>Thermal parameters ( $\times 10^4$ ) are of the form  $T = \exp(-\sum_{i,j} h_i h_j \beta_{ij})$ .

gation of the intergrown sanidine along *a* (see Table 1). The Ribbe and Gibbs (1969) equation estimates a slight ordering of Al into the T<sub>1</sub> site ( $t_1 = 0.28\text{Al}$ ) and estimates a total Al content ( $t_1 + t_2$ ) of 1.03. T-O and K-O interatomic distances in this structure are given in Table 4.

#### The high-albite structure

The structure of the intergrown high-albite phase is significantly different from that of a synthetic, non-intergrown albite (composition  $\text{Na}_{0.98}\text{K}_{0.01}\text{Ca}_{0.01}\text{AlSi}_3\text{O}_8$ , 24°C) reported by Prewitt *et al.* (1976). This difference manifests itself as a lesser deviation from monoclinic symmetry in the intergrown phase. This is in large part accounted for by the higher K content of the high albite in this study, although partial coherency of the high albite with the monoclinic sanidine is expected to have a similar effect.

As in the case of the sanidine, no study of a non-intergrown high-albite structure similar in composition to the albite in this study has been reported to date, which restricts discussion of the effect of intergrowth to general features. The mean alkali-oxygen distance of the nine nearest oxygen atoms is within 0.002Å of that reported by Prewitt *et al.* (1976), although individual M-O distances differ by as much as 0.125Å (for M-O<sub>Dm</sub>, Table 4). The mean M-O distance predicted by Fenn and Brown's work for the observed high-albite composition is 0.03Å larger than that observed.

The T<sub>10</sub>-O<sub>Co</sub> and T<sub>1m</sub>-O<sub>Cm</sub> bonds in the intergrown phase are 0.022 and 0.027Å longer, respectively, than in the non-intergrown phase. These differences are significantly larger than would be expected solely due to the effect of the different Na/K ratio on these bonds<sup>5</sup>. This elongation of the T<sub>10</sub>-O<sub>Co</sub> and T<sub>1m</sub>-O<sub>Cm</sub> bonds, which are essentially parallel to the *b* axis, contributes roughly 80 percent of the elongation of the *b* axis indicated in Table 1. A further consequence of this elongation is an average T-O distance which yields a total Al content (as predicted by the Ribbe and Gibbs equation) of 1.13, thereby invalidating estimates of the degree of Al-Si ordering in the intergrown high albite.

<sup>5</sup> For example, the T<sub>10</sub>-O<sub>Co</sub> distance in the non-intergrown sanidine structure of Phillips and Ribbe (1973) is 0.020Å longer than that of the non-intergrown high albite, which contains 84 mole percent more Na than the sanidine. The T<sub>10</sub>-O<sub>Co</sub> distance in the intergrown high albite is 0.027Å longer than that of the non-intergrown high albite, which has only 21 mole percent more Na than the intergrown phase.

Table 4. T-O and M-O interatomic distances (in Å) in the intergrown phases

	Sanidine	High Albite
T <sub>10</sub> - O <sub>A1</sub>	1.653(1) <sup>1</sup>	1.651(5)
O <sub>Bo</sub>	1.643(2)	1.651(4)
O <sub>Co</sub>	1.651(1)	1.660(5)
O <sub>Do</sub>	1.657(1)	1.663(4)
mean	1.651	1.656
T <sub>1m</sub> - O <sub>A1</sub>	1.653(1)	1.662(5)
O <sub>Bm</sub>	1.643(2)	1.640(5)
O <sub>Cm</sub>	1.651(1)	1.671(4)
O <sub>Dm</sub>	1.657(1)	1.654(4)
mean	1.651	1.657
T <sub>20</sub> - O <sub>A2</sub>	1.644(1)	1.656(4)
O <sub>Bo</sub>	1.629(2)	1.641(4)
O <sub>Cm</sub>	1.642(1)	1.623(4)
O <sub>Dm</sub>	1.636(1)	1.631(4)
mean	1.638	1.638
T <sub>2m</sub> - O <sub>A2</sub>	1.644(1)	1.656(4)
O <sub>Bm</sub>	1.629(2)	1.628(5)
O <sub>Co</sub>	1.642(1)	1.638(4)
O <sub>Do</sub>	1.636(1)	1.648(4)
mean	1.638	1.643
M - O <sub>A(1000)</sub>	2.882(1)	2.607(7)
O <sub>A(100c)</sub>	2.882(1)	2.671(7)
O <sub>A(2000)</sub>	2.676(2)	2.357(4)
O <sub>B(000c)</sub>	3.014(2)	2.659(7)
O <sub>B(m00c)</sub>	3.014(2)	3.083(9)
O <sub>E(02z0)</sub>	3.131(1)	3.289(7)
O <sub>C(m2z0)</sub>	3.131(1)	2.996(7)
O <sub>D(0000)</sub>	2.931(2)	2.610(7)
O <sub>D(m000)</sub>	2.931(2)	3.008(9)
mean	2.955	2.809

<sup>1</sup>Numbers in parentheses are *e.s.d.*'s (1σ) in the least significant digits.

## Discussion

### Coherency strain

Robin (1974) and Tullis (1975) have calculated the elastic strain induced by perfect coherency between intergrown *monoclinic* alkali feldspars of different compositions. Knowledge of this strain is important because the compositions of submicroscopically in-

tergrown alkali feldspars are often estimated from observed  $a$  and  $d_{201}$  values and nomograms derived from cell parameters of unstrained phases (*cf.* Stewart and Wright, 1974). Intergrown phases are commonly strained, so compositional estimates based on such nomograms are incorrect.

The compositional and structural data from our study provide the first test of these theoretical models used to predict strain and the effects of strain on the compositional estimates of intergrown alkali feldspar lamellae. Because experimentally-determined cell dimensions for unstrained feldspars with the same compositions as our intergrown phases are not available, we have used as a reference state for strain analysis cell dimensions calculated from the regression equations of Luth and Querol-Suñé (1970) for the Orville (1967) synthetic sanidine-high albite series (Table 1). The major and minor axes of the strain tensor calculated with Ohashi and Finger's (1973) STRAIN program are essentially parallel to the  $a$  and  $b$  cell axes, respectively. Further references to strain will therefore be made in terms of the components along the direct cell axes rather than the axes of the strain ellipsoid.

The cell dimensions and crystal structures of the intergrown phases reported in this study represent average structures of the phases. If strain due to partial coherency decreases away from the phase boundary, the structures at the boundary may be quite different from those at the center of the lamellae. Robin (1974) has shown that if the lamellae are elastic, perfectly coherent, and have large aspect ratios, strain is uniform throughout the lamellae. However, the very large r.m.s. amplitudes of atomic vibration found in the refinements of the intergrown structures suggest that structural distortion varies within the lamellae. These amplitudes are almost an order of magnitude larger than the dimensional mismatch of the average lattices of the intergrown phases, and are more likely due to a space-averaged disorder caused by a variation in strain than to true thermal motion. This interpretation implies that strain is not uniform throughout the lamellae.

The  $b$  and  $c$  cell dimensions of the intergrown high albite are more nearly equal to those of the intergrown sanidine than would be the case for the two non-intergrown phases. Therefore, the sanidine and high-albite phases are inferred to be strained and partially coherent in the intergrowth plane,  $\sim(\bar{6}01)$ . Comparison of the observed and calculated values of  $b$  and  $c$  shown in Table 1 suggests that the volumetrically-dominant sanidine phase is less strained

than the high-albite phase, although comparison of  $V$  suggests the reverse to be true. The  $a$  axes of both phases are highly strained. The strain in the  $a$  direction predicted by the models of Robin (1974) and Tullis (1975) for both phases is less than half of that actually observed. The observed volumetric strain is positive in the sanidine phase and negative in the high-albite phase, exactly the reverse of theoretical predictions. Furthermore, both models predict a lesser magnitude of volumetric strain in the volumetrically-dominant phase, in this case the sanidine, and again the opposite is observed.

The most probable reason for the discrepancy between our observations of the strain of the phases of cryptoperthite and the predictions of the models of Robin (1974) and Tullis (1975) is that our natural system consists of a monoclinic phase and a twinned triclinic phase, whereas both models are derived for a system of two untwinned monoclinic phases. The inversion of the high-albite phase from a monoclinic to a triclinic structure (*cf.* Smith, 1974, pp. 301–305) probably allows some relaxation of the strain in that phase, and also produces a different set of stresses on the sanidine than exist when both phases are monoclinic. Our results demonstrate that models of strain derived for coherent monoclinic feldspars are not generally valid, even as approximations, for strain in intergrowths of a monoclinic and a triclinic feldspar, and that predicted compositions based on cell dimensions corrected for these strain effects are also invalid (Table 5).

Table 5. Estimates of the compositions of the phases in the cryptoperthite of this study

Sanidine	High Albite	Comments
0.65(1) <sup>1</sup>	0.22(2) <sup>2</sup>	Composition determined in this study.
0.85	-0.24 <sup>2</sup>	Estimated <sup>3</sup> from sanidine cell volume.
0.88	-0.31 <sup>2</sup>	Estimated <sup>3</sup> from sanidine $a$ cell edge.
0.68 <sup>2</sup>	0.16	Estimated <sup>3</sup> from high albite cell volume.
0.75 <sup>2</sup>	-0.01	Estimated <sup>3</sup> from high albite $a$ cell edge.
0.92	0.14	Estimated using method of Robin (1974).
0.79	0.07	Estimated using method of Tullis (1975).

<sup>1</sup>Compositions are given as mole fraction of the formula unit  $KAlSi_3O_8$ .

<sup>2</sup>These values computed by mass balance, based on bulk composition of  $K_{0.51}Na_{0.48}Ca_{0.01}AlSi_3O_8$ , a mole fraction of the sanidine phase in the crystal of 0.68, and the composition estimated for the other phase.

<sup>3</sup>Composition estimates from cell dimensions calculated from the regression equations of Luth and Querol-Suñé (1970) for the Orville (1967) sanidine-high albite series.

Another possible contribution to the discrepancy between the theoretical calculations and the observed results is that neither model treats thermal strain effects. Thermal expansion of feldspars does vary significantly with composition (Stewart and von Limbach, 1967; Brown and Fenn, 1975; Prewitt *et al.*, 1976). The intergrowth boundary between the phases is established at temperatures on the order of 400–550° higher than room temperature at which cell dimensions are usually measured. Hence, differential thermal contraction might contribute an additional strain to systems studied at room temperature.

#### Solvi and exsolution

Solvi for coherent alkali feldspar systems have been calculated by Robin (1974) for a pressure of 1 kbar and measured by Sipling and Yund (1976) at a pressure of 1 bar<sup>6</sup>. These solvi and the equilibrium solvus calculated from the Margules parameters determined by Luth *et al.* (1974) are shown in Figure 3. Both calculated solvi have been extrapolated to 200 bars, the estimated pressure at which the cryptoperthite in the present study cooled (J. O'Brient, personal communication). Within experimental error, the compositions of the phases in the present study lie on the experimental coherent solvus of Sipling and Yund (1976) at a temperature of  $465 \pm 20^\circ\text{C}$  and do not, at any temperature, lie on the other two solvi (Fig. 3).

Smith (1974, p. 305) has used Kroll and Bambaue's (1971) data to construct the phase boundary between monoclinic and triclinic sodic feldspars, which is also shown in Figure 3. This phase boundary intersects the coherent solvus of Sipling and Yund in the temperature range  $465 \pm 20^\circ\text{C}$ , the same temperature at which our observed compositions lie on that solvus. The compositions observed in our study may be explained by the following exsolution path, illustrated in Figure 3.

As the crystal of bulk composition  $\text{Or}_{0.51}\text{An}_{0.01}\text{Ab}_{0.48}$  cooled from  $\sim 570^\circ$  to  $\sim 465^\circ\text{C}$ , coherent monoclinic phases with compositions lying on the coherent solvus exsolved. At  $\sim 465^\circ\text{C}$  the sodic phase inverted to triclinic symmetry and pericline twinned. Consequently coherency with the monoclinic potassic phase was reduced. After this reduc-

<sup>6</sup> The compositions for the Sipling-Yund solvus were determined using cell dimensions corrected for strain effects by Tullis's (1975) strain model. Although we question the validity of this model for an intergrowth of a triclinic sodic and a monoclinic potassic feldspar, we have no reason to doubt its validity for an intergrowth of two monoclinic feldspars.

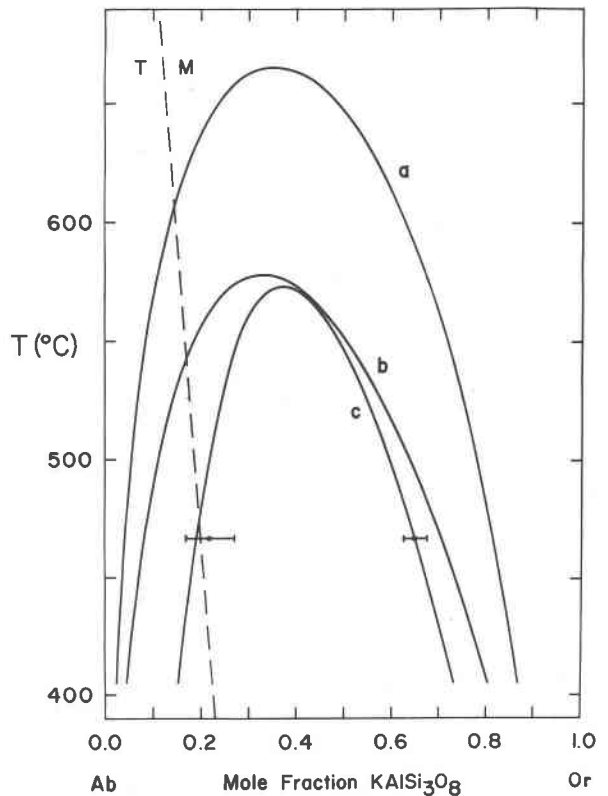


Fig. 3. Curve *a* is the equilibrium solvus at 200 bar, curve *b* is the coherent solvus at 200 bar calculated by Robin (1974), curve *c* is the coherent solvus at 1 bar experimentally determined by Sipling and Yund (1976). The dashed line is the monoclinic-triclinic inversion boundary based on the data of Kroll and Bambaue (1971). The compositions of the phases in this study are shown plotted on curve *c* with  $2\sigma$  error bars.

tion of coherency, metastable equilibrium as defined by the coherent solvus can no longer exist, and the only equilibrium which does exist is between phases whose compositions lie on the equilibrium solvus. Because the system is presumably closed and the composition of the potassic phase lies outside the chemical spinodal at  $465^\circ\text{C}$ , further phase separation will not, in theory, occur without nucleation and growth of phases whose compositions lie on the equilibrium solvus. At these relatively low temperatures nucleation and growth is kinetically inhibited. Thus phases whose compositions lie on the coherent solvus at  $465^\circ\text{C}$  will tend to persist metastably when cooling is complete, accounting for the compositions observed in this study.

#### Acknowledgments

We thank Dr. C. M. Taylor (Stanford University) for performing the microprobe analysis of the cryptoperthite crystal used in this study, Dr. H.-R. Wenk (U.C. Berkeley) for ion-thinning an

oriented section of our cryptoperthite for TEM work, and Ms. C. Gosnell (U.C. Berkeley) for helping us obtain the TEM micrograph. Dr. V. C. Kelley (University of New Mexico) kindly provided the cryptoperthite specimen. We gratefully acknowledge Drs. P. M. Fenn and M. P. Taylor (Stanford University) and Dr. J. Tullis (Brown University) for helpful discussions and for critical readings of an early version of the manuscript. Standard Oil of California generously allowed us to use their IBM 370/168 computer for many of the calculations. This study was supported by NSF grant EAR-74-03056-A01. One of us (KDK) received support as a National Science Foundation Graduate Fellow.

### References

- Brown, G. E. and P. M. Fenn (1975) High temperature structural study of an homogeneous, intermediate composition alkali feldspar (abstr.). *Geol. Soc. Am. Abstracts with Programs*, 7, 1012.
- Corfield, R., R. J. Dodens and J. A. Ibers (1967) The crystal and molecular structure of nitridodichlorobis(triphenylphosphine) rhenium(V),  $\text{ReNCl}_2(\text{P}(\text{C}_6\text{H}_5)_3)_2$ . *Inorg. Chem.*, 6, 197-204.
- Cromer, D. T. and J. B. Mann (1968) X-ray scattering factors computed from numerical Hartree-Fock wave functions. *Acta Crystallogr.*, A24, 321-324.
- De Meulenaer, J. and H. Tompa (1965) The absorption correction in crystal structure analysis. *Acta Crystallogr.*, 19, 1014-1018.
- Fenn, P. M. and G. E. Brown (1977) Crystal structure of a synthetic, compositionally intermediate, hypersolvus alkali feldspar. *Z. Kristallogr.*, 145, 124-145.
- Finger, L. W. and E. Prince (1975) A system of FORTRAN IV computer programs for crystal structure computations. *NBS Technical Note 854*, U.S. Department of Commerce, Washington.
- Kroll, H. and H. U. Bambauer (1971) The displacive transformation of (K,Na,Ca) feldspars. *Neues Jahrb. Mineral., Monatsh.*, 413-416.
- Kuellmer, F. J. (1954) *Geologic Section of the Black Range at Kingston, New Mexico*. New Mexico Bur. Mines Bull. 33.
- Luth, W. C., R. F. Martin and P. M. Fenn (1974) Peralkaline alkali feldspar solvi. In W. S. MacKenzie and J. Zussman, Eds., *The Feldspars*, p. 297-312. Manchester University Press, Manchester, England.
- and F. Querol-Suñé (1970) An alkali feldspar series. *Contrib. Mineral. Petrol.*, 25, 25-40.
- Ohashi, Y. and L. W. Finger (1973) Lattice deformations in feldspars. *Carnegie Inst. Wash. Year Book*, 72, 569-573.
- Orville, P. M. (1967) Unit-cell parameters of the microcline-low albite and the sanidine-high albite solid solution series. *Am. Mineral.*, 52, 55-86.
- Owen, D. C. and J. D. C. McConnell (1974) Spinodal unmixing in an alkali feldspar. In W. S. MacKenzie and J. Zussman, Eds., *The Feldspars*, p. 424-439. Manchester University Press, Manchester, England.
- Phillips, M. W. and P. H. Ribbe (1973) The structures of monoclinic potassium-rich feldspars. *Am. Mineral.*, 58, 263-270.
- Prewitt, C. T., S. Sueno and J. J. Papike (1976) The crystal structures of high albite and monalbite at high temperatures. *Am. Mineral.*, 61, 1213-1225.
- Ribbe, P. H. and G. V. Gibbs (1969) Statistical analysis of mean Al-Si-O bond distances and the aluminum content of tetrahedra in feldspars. *Am. Mineral.*, 54, 85-94.
- and — (1975) The crystal structure of a strained intermediate microcline in cryptoperthitic association with low albite (abstr.). *Geol. Soc. Am. Abstracts with Programs*, 7, 1245.
- , H. D. Megaw, W. H. Taylor, R. B. Ferguson and R. J. Traill (1969) The albite structures. *Acta Crystallogr.*, B25, 1503-1518.
- Robin, P.-Y. F. (1974) Stress and strain in cryptoperthite lamellae and the coherent solvus of alkali feldspars. *Am. Mineral.*, 59, 1299-1318.
- Sipling, P. J. and R. A. Yund (1976) Experimental determination of the coherent solvus for sanidine-high albite. *Am. Mineral.*, 61, 897-906.
- Smith, J. V. (1974) *Feldspar Minerals, Vol. 1, Crystal Structure and Physical Properties*. Springer-Verlag, New York.
- Stewart, D. B. and D. von Limbach (1967) Thermal expansion of low and high albite. *Am. Mineral.*, 52, 389-413.
- and T. L. Wright (1974) Al/Si order and symmetry of natural alkali feldspars, and the relationship of strained cell parameters to bulk composition. *Bull. Soc. fr. Mineral. Cristallogr.*, 97, 356-377.
- Tullis, J. (1975) Elastic strain effects in coherent perthitic feldspars. *Contrib. Mineral. Petrol.*, 49, 83-91.
- Yund, R. A. (1974) Coherent exsolution in the alkali feldspars. In A. W. Hoffmann, B. J. Giletti, H. S. Yoder, Jr. and R. A. Yund, Eds., *Geochemical Transport and Kinetics*, p. 173-183. Academic Press, New York.

*Manuscript received, November 28, 1977; accepted for publication, April 11, 1978.*